Available online at www.sciencedirect.com
ScienceDirect
International Journal of Thermal Sciences 48 (2009) 1161–1175
International Journal of Thermal Sciences
www.elsevier.com/locate/ijts

# Entropy analysis due to conjugate-buoyant flow in a right-angle trapezoidal enclosure filled with a porous medium bounded by a solid vertical wall

Yasin Varol [a], Hakan F. Oztop [b], Ioan Pop [c,*]

[a] *Department of Mechanical Education, Firat University, 23119 Elazig, Turkey*
[b] *Department of Mechanical Engineering, Firat University, 23119 Elazig, Turkey*
[c] *Faculty of Mathematics, University of Cluj, CP 253, 3400 Cluj, Romania*

Received 8 February 2008; received in revised form 6 August 2008; accepted 6 August 2008

Available online 29 August 2008

**Abstract**

Entropy generation due to buoyancy induced convection and conduction in a right angle trapezoidal enclosure filled with fluid saturated porous medium has been performed numerically. Left vertical solid wall of the trapezoidal enclosure has a finite thickness and conductivity. The outside temperature of the solid wall is higher than that of inclined wall, while horizontal walls are adiabatic. The governing Darcy and energy equations are solved numerically using a finite difference method. The study is performed for different governing parameters including the Rayleigh number ($50 \leqslant Ra \leqslant 1000$), inclination angle of the inclined wall of the enclosure ($\gamma = 35°$, $45°$ and $60°$), dimensionless thickness of the solid vertical wall ($S = 0.05$, 0.1 and 0.2), and thermal conductivity ratio ($k = 0.1$, 1.0 and 10). Entropy generation is calculated by using the obtained velocities and temperature distributions from the computer code. Results are presented for the Bejan number, local and mean Nusselt numbers, streamlines, isotherms, iso-Bejan lines and entropy generation contours. It is found that the most important parameters on heat transfer and fluid flow are thermal conductivity ratio and dimensionless thickness of the solid wall of the enclosure. Thus, these parameters also generate entropy for the whole system. It is also found that increasing the Rayleigh number decreases the Bejan number; however, heat transfer is an increasing function of Rayleigh number.
© 2008 Elsevier Masson SAS. All rights reserved.

*Keywords:* Conjugate trapezoidal enclosure; Entropy generation; Porous medium; Natural convection; Numerical results

## 1. Introduction

Applications of porous media include utilization of geothermal energy, design of packed bed reactors, oil recovery, insulation of buildings and cold storage, drying processes, energy storage systems, solar collectors, heat exchangers, transpiration cooling, powder metallurgy, solidification of binary alloys, agricultural engineering, etc. These are some of applications and the most of studies in porous media have been recently excellently reviewed by Nield and Bejan [1], Ingham and Pop [2], Ingham et al. [3] and Vafai [4].

The study for an inclined trapezoidal enclosure at different inclination angles filled with a viscous fluid has been analyzed by Lee [5]. He made a numerical analysis to solve the natural convection heat transfer in an inclined trapezoidal enclosure filled with viscous fluid for different Prandtl numbers $Pr$ using body-fitted coordinate systems. It was shown that for $Ra > 10^4$ and $Pr > 0.1$, the heat transfer, in a trapezoidal enclosure with two symmetrical, inclined sidewalls of moderate aspect ratios, is a strong function of the orientation angle of the cavity. Kumar and Kumar [6] used parallel computation technique to analyze the natural convection heat transfer in a trapezoidal enclosure filled with a porous medium. The short bottom and the long top walls are taken adiabatic, while the sloping walls are differentially heated. They showed that the inclination of the side wall substantially affects the flow and temperature distributions. Baytas and Pop [7] solved to Darcy and energy equation in cylindrical coordinates using ADI method to analyze natural convection in a trapezoidal enclosure filled with a porous medium. It has been observed that up to Rayleigh number $Ra = 100$, a conduction-dominated regime prevails, and afterwards a two-cellular convective flow regime takes place at the

* Corresponding author. Tel.: +40 264 594315; fax: +40 264 591906.
*E-mail address:* pop.ioan@yahoo.co.uk (I. Pop).

1290-0729/$ – see front matter © 2008 Elsevier Masson SAS. All rights reserved.
doi:10.1016/j.ijthermalsci.2008.08.002

**Nomenclature**

| | | |
|---|---|---|
| $Be$ | Bejan number | |
| $g$ | gravitational acceleration | m/s$^2$ |
| $Gr$ | Grashof number | |
| $H$ | height of the enclosure | m |
| $k_f$ | thermal conductivity of the fluid | W/m K |
| $k_s$ | thermal conductivity of the solid | W/m K |
| $k$ | thermal conductivity ratio ($k_s/k_f$) | |
| $K$ | permeability of the porous medium | m$^2$ |
| $L$ | length of bottom wall of the enclosure | m |
| $Nu$ | local Nusselt number | |
| $Nu_m$ | mean Nusselt number | |
| $N_s$ | entropy generation number | |
| $Pr$ | Prandtl number | |
| $Ra$ | Rayleigh number for a porous medium | |
| $S'$ | thickness of the solid wall | m |
| $S$ | dimensionless thickness of the solid wall | |
| $S'''_{\text{gen}}$ | entropy generation rate per unit volume | W/m$^3$ K |
| $T$ | temperature | K |
| $T_0$ | $(T_h + T_c)/2$ | K |
| $u$, $v$ | dimensional axial and radial velocities | m/s |
| $x$, $y$ | dimensional coordinates | m |
| $U$, $V$ | dimensionless axial and radial velocities | |
| $X$, $Y$ | dimensionless coordinates | |
| $\Delta T$ | temperature difference $(T_h - T_c)$ | K |

*Greek letters*

| | | |
|---|---|---|
| $\alpha_m$ | effective thermal diffusivity of the porous medium | m$^2$/s |
| $\beta$ | coefficient of thermal expansion | K$^{-1}$ |
| $\gamma$ | inclination angle of inclined wall | deg |
| $\theta$ | non-dimensional temperature | |
| $\upsilon$ | kinematic viscosity | m$^2$/s |
| $\mu$ | dynamic viscosity | kg/m s |
| $\phi$ | irreversibility distribution ratio | |
| $\psi$ | stream function | m$^2$/s |
| $\Psi$ | non-dimensional stream function | |

*Subscripts*

| | |
|---|---|
| $c$ | cold |
| $f$ | fluid |
| $h$ | hot |
| $s$ | solid |

tilt angle 165°. Moukalled and Acharya [8] studied the conjugate natural convection in a trapezoidal enclosure with a divider attached to the inclined wall and filled with a viscous fluid. Moukalled and Darwish [9] made a numerical work on natural convection in a partitioned trapezoidal cavity using the special momentum-weighted interpolation method (MWIM). They used conductive partition and showed that the presence of baffles decrease heat transfer as high as 70%. Other similar studies on natural convection in trapezoidal cavities can be found in Boussaid et al. [10], Van Der Eyden et al. [11], Kumar [12], Papanicolaou and Belessiotis [13], Varol et al. [14], Peric [15] and Hammami et al. [16]. It should be mentioned that in many practical situations, especially those concerned with the design of thermal insulation, conduction in the walls can have an important effect on the natural convection flow in the enclosure.

Minimization of entropy generation is a method for modeling and optimizing of energy systems. It results in from the analysis of the second law of thermodynamics. In earlier studies related to the natural convection problem in triangular isosceles enclosures, only the first-law of thermodynamics was used. However, the method of entropy generation combines from the start the most important parameters of thermodynamics, heat transfer and fluid mechanics. Fundamentals of entropy generation are presented by Bejan [17], San et al. [18], Rosen [19] and Narusawa [20]. Mourad et al. [21] investigated the entropy production due to heat transfer, mass transfer and fluid friction for the steady state laminar double diffusive convection in an inclined square enclosure. Their results show that the total entropy production increases with the thermal Grashof number and the buoyancy ratio for moderate values of the Lewis numbers. Erbay et al. [22] numerically studied the entropy production during the transient laminar natural convection in a square enclosure which is heated either completely or partially from the left-side wall and cooled from the opposite wall. They found that the active sites in the completely heated case are at the left bottom corner of the heated wall and the right top corner of the cooled wall at the same magnitudes. In the case of partial heating, the active site is observed at the top corner of the heated section. Yilbas et al. [23] analyzed the entropy production due to natural convection in an enclosure heated from bottom and cooled from the top wall with insulated vertical walls. Baytas [24] made a study on the entropy production in an inclined enclosure. He showed that entropy production strongly depends on the inclination angle of the enclosure. Magherbi et al. [25] analyzed the time dependent entropy production in a differentially heated enclosure. Magnetohydrodynamic (MHD) free convection and entropy production were investigated by Mahmud and Fraser [26] who showed that both Rayleigh and Hartmann numbers are strongly effective parameters on flow, heat transfer and entropy production. However, the number of studies of entropy generation in a conduction-convection (conjugate) system is extremely limited in the literature. In this context, Ruocco [27] made a study to analysis the entropy generation due to jet impingement onto a plate and Varol et al. [28] performed this analysis for a thick walled cavity.

Our principal aim in this study is to present theoretical results for entropy generation due to conjugate natural convection heat transfer in a right-angle trapezoidal enclosure filled with a porous medium for different Rayleigh numbers, inclination angles of the inclined wall of the cavity, thicknesses of the solid vertical wall and thermal conductivity ratios. As seen from the above literature survey the entropy generation due to natural convection thick walled right-angle porous trapezoidal enclosure has not been studied by researchers yet. Therefore,

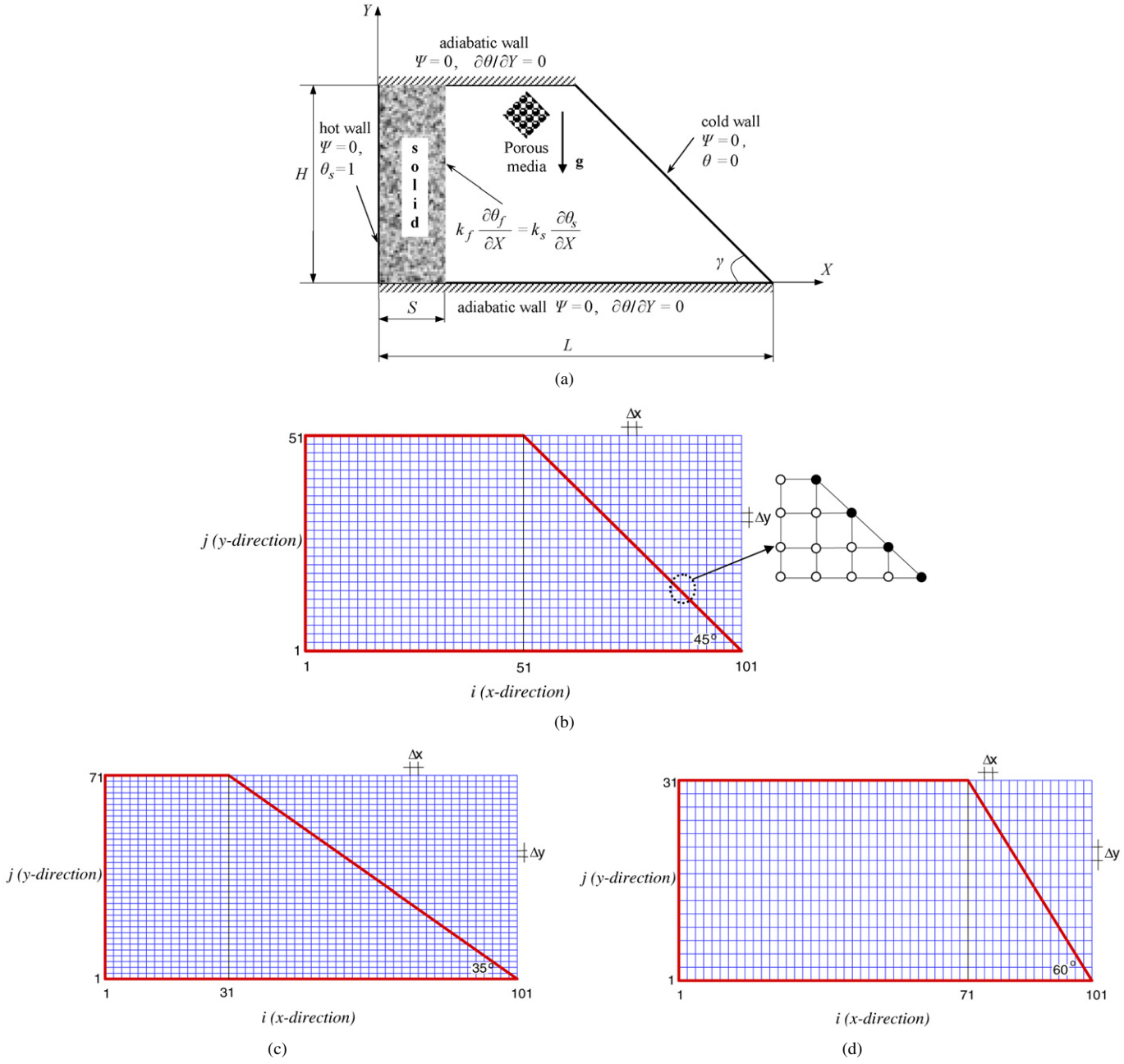


Fig. 1. (a) Schematical configuration with boundary conditions of right-angle trapezoidal cavity with thick left wall, (b) grid distributions for $\gamma = 45°$, (c) grid distributions for $\gamma = 35°$, (d) grid distributions for $\gamma = 60°$.

the present study is important for understanding the relationship between the solid and the fluid saturated porous medium within the enclosure which can be observed in underground or geological applications. It is also important to geophysics and environmental sciences.

## 2. Physical model

Physical model for the present study is shown in Fig. 1(a) with coordinates and boundary conditions. It is a right-angle trapezoidal enclosure filled with a porous medium. The inclination angle of inclined wall is shown by $\gamma$. The model includes a thick vertical wall which is heated ($T_h$) from the outside with an isothermal heater and its inclined wall is cooled ($T_c$), while the top and bottom walls are insulated. The height of the enclosure is denoted by $H$ and its bottom length is given by $L$. It is noticed that the analysis is made for the ratio $H/L = 0.5$ and $L = 1$ for all cases. But the change of the length of top wall depends on inclination angle of the enclosure. The thickness of the solid vertical wall is denoted by $S'$.

## 3. Analysis

### 3.1. Governing equations

The following assumptions are made to obtain the governing equations of the present geometry: the properties of the fluid

and the porous medium are constant; the cavity walls are impermeable; the Boussinesq approximation and the Darcy law model are valid; and the viscous drag and inertia terms of the momentum and energy equations are neglected. With these assumptions, the dimensional governing equations of continuity, momentum and energy can be written as follows:

$$\frac{\partial u}{\partial x}+\frac{\partial v}{\partial y}=0 \tag{1}$$

$$\frac{\partial u}{\partial y}-\frac{\partial v}{\partial x}=-\frac{g\beta K}{\upsilon}\frac{\partial T_f}{\partial x} \tag{2}$$

$$u\frac{\partial T_f}{\partial x}+v\frac{\partial T_f}{\partial y}=\alpha_m\left(\frac{\partial^2 T_f}{\partial x^2}+\frac{\partial^2 T_f}{\partial y^2}\right) \tag{3}$$

and the energy equation for the solid vertical wall is:

$$\frac{\partial^2 T_s}{\partial x^2}+\frac{\partial^2 T_s}{\partial y^2}=0 \tag{4}$$

where $x$ and $y$ are the Cartesian coordinates measured along the bottom wall and along the vertical hot wall of the cavity, respectively, $u$ and $v$ are the velocity components along $x$ and $y$ axes, $T_f$ is the fluid temperature, $g$ is the acceleration due to gravity, $T_s$ is the temperature of the solid vertical wall, $K$ is the permeability of the porous medium, $\alpha_m$ is the effective thermal diffusivity of the porous medium, $\beta$ is the thermal expansion coefficient and $\upsilon$ is the kinematic viscosity. Introducing the stream function $\psi$ defined as

$$u=\frac{\partial \psi}{\partial y},\qquad v=-\frac{\partial \psi}{\partial x} \tag{5}$$

Eqs. (1)–(4) can be written in non-dimensional form as

$$\frac{\partial^2 \Psi}{\partial X^2}+\frac{\partial^2 \Psi}{\partial Y^2}=-Ra\frac{\partial \theta_f}{\partial X} \tag{6}$$

$$\frac{\partial \Psi}{\partial Y}\frac{\partial \theta_f}{\partial X}-\frac{\partial \Psi}{\partial X}\frac{\partial \theta_f}{\partial Y}=\frac{\partial^2 \theta_f}{\partial X^2}+\frac{\partial^2 \theta_f}{\partial Y^2} \tag{7}$$

for the fluid-saturated porous medium and

$$\frac{\partial^2 \theta_s}{\partial X^2}+\frac{\partial^2 \theta_s}{\partial Y^2}=0 \tag{8}$$

for the solid vertical wall, respectively. Here $Ra=g\beta K(T_h-T_c)L/\alpha_m\upsilon$ is the Rayleigh number for the porous medium and the non-dimensional quantities are defined as

$$X=\frac{x}{L},\qquad Y=\frac{y}{L},\qquad (U,V)=\frac{(u,v)L}{\alpha_m},\qquad \Psi=\frac{\psi}{\alpha_m}$$
$$\theta_f=\frac{T_f-T_c}{T_h-T_c},\qquad \theta_s=\frac{T_s-T_c}{T_h-T_c} \tag{9}$$

### 3.2. Boundary conditions

The boundary conditions of Eqs. (6)–(8) are:

for all solid boundaries

$$\Psi=0 \tag{10a}$$

on the vertical wall (hot), $0\leqslant Y\leqslant 0.5$

$$\theta_s=1 \tag{10b}$$

on the bottom wall (adiabatic), $0\leqslant X\leqslant 1$

$$\frac{\partial \theta_f}{\partial Y}=0 \tag{10c}$$

on the top wall (adiabatic)

$$\frac{\partial \theta_f}{\partial Y}=0 \tag{10d}$$

on the inclined wall (cold)

$$\theta_f=0 \tag{10e}$$

for the interface between solid vertical wall and porous medium,

$$k_f\frac{\partial \theta_f}{\partial X}=k_s\frac{\partial \theta_s}{\partial X} \tag{10f}$$

Physical quantities of interest in this problem are the local Nusselt number $Nu$ and the mean $Nu_m$ Nusselt number, which are given by

$$Nu=\left(-\frac{\partial \theta_f}{\partial X}\right)_{X=S} \tag{11a}$$

$$Nu_m=\frac{1}{H}\int_0^H Nu\,dy \tag{11b}$$

for the interface between the solid vertical wall and porous medium.

## 4. Entropy generation

The non-equilibrium conditions due to the exchange of energy and momentum, within the fluid-saturated porous medium and at the solid boundaries, cause a continuous entropy generation in the flow field of the porous enclosure. This entropy generation is due to the irreversible nature of heat transfer and viscosity effects, within the fluid and at the solid boundaries. From the known temperature and velocity fields, volumetric entropy generation can be calculated from the equation (Baytas [24]),

$$S'''_{\text{gen}}=\frac{k_f}{T_0^2}(\nabla T)^2+\frac{\mu}{KT_0}(u^2+v^2) \tag{12}$$

By using the same dimensionless parameters given in Eq. (9), the dimensionless entropy generation number $N_s$ can be expressed as

$$N_s=\left[\left(\frac{\partial \theta}{\partial X}\right)^2+\left(\frac{\partial \theta}{\partial Y}\right)^2\right]+\phi\left[\left(\frac{\partial \Psi}{\partial Y}\right)^2+\left(\frac{\partial \Psi}{\partial X}\right)^2\right] \tag{13}$$

In this equation, $\phi$ is defined as the irreversibility distribution ratio

$$\phi=\frac{\mu T_0}{k_f}\left(\frac{\alpha_m^2}{K(\Delta T)^2}\right) \tag{14}$$

and its value is taken equal to $10^{-2}$ in all calculations. We notice that Eq. (13) consists of two parts. The first part (first square bracketed term) is the irreversibility due to finite temperature gradient and generally termed as the heat transfer irreversibility (HTI). The second part (second square bracketed term) is the

Table 1
Optimal grid dimensions for different inclination angles of the inclined wall at $k = 1.0$, $S = 0.1$ and $Ra = 1000$

| Inclination angle of the inclined wall ($\gamma$) | Grid dimension ($X$ by $Y$) | Mean Nusselt number ($Nu_m$) |
|---|---|---|
| 35° | 51 × 36 | 5.176 |
| | 101 × 71 | 5.603 |
| | 151 × 106 | 5.881 |
| | 201 × 141 | 5.752 |
| 45° | 51 × 26 | 5.096 |
| | 81 × 41 | 5.244 |
| | 101 × 51 | 5.328 |
| | 151 × 76 | 5.378 |
| 60° | 51 × 16 | 4.814 |
| | 101 × 31 | 5.067 |
| | 151 × 46 | 5.188 |
| | 201 × 61 | 5.238 |

contribution of fluid friction irreversibility (FFI) to entropy generation. The overall entropy generation, for a particular problem, is an internal competition between HTI and FFI. Usually, free convection problems, at low and moderate Rayleigh numbers, are dominated by the heat transfer irreversibility. Entropy generation number ($N_s$) is important for generating entropy profiles or maps but fails to give any idea whether fluid friction or heat transfer are dominate. The two parameters, namely, the irreversibility distribution ratio ($\phi$) and Bejan number ($Be$) are achieving an increasing popularity among the researchers of the Second-Law of Thermodynamics. Finally, it is noticed that Bejan number ($Be$), which is the ratio of heat transfer irreversibility to the entropy production number ($N_s$), can be mathematically expressed as

$$Be = \frac{\left[\left(\frac{\partial\theta}{\partial X}\right)^2 + \left(\frac{\partial\theta}{\partial Y}\right)^2\right]}{N_s} \tag{15}$$

## 5. Numerical procedure

Eqs. (6)–(8) subject to the boundary conditions 10(a)–(f) are integrated numerically using the finite-difference method. Numerical simulations were carried out systematically in order to determine the effects of four main parameters of the problem, namely: Rayleigh number $Ra$, thermal conductivity ratio $k$ $(= k_s/k_f)$, dimensionless thickness of the solid vertical wall $S$ $(= S'/L)$ and the inclination angle of the inclined wall of the enclosure $\gamma$ on the flow and heat transfer characteristics. The solution domain consists of grid points at which equations are applied. Table 1 shows optimal grid dimensions for different inclination angles $\gamma$. To obtain a grid-independent solution, different grid dimensions were obtained for each $\gamma$ and chosen grid dimensions were given inside dashed ellipsoid. As shown in Table 1, 101 × 71 grid dimensions were chosen for 35°, 101 × 51 grid dimensions for 45° and 101 × 31 grid dimensions were chosen for 60°. The inclined wall was approximated with staircase-like zigzag lines [29,30]. As indicated above that the ratio of $H/L$ is equal to 0.5 for whole study and inclination angle belongs to the inclined wall. Fig. 1(b)–(d) gives the grid distributions for$\gamma = 45°$, $\gamma = 35°$ and $\gamma = 60°$, respectively. As shown in these figures, the bold nodes are the boundary nodes and they have Dirichlet boundary conditions. Values of internal nodes are calculated using boundary values via central finite-difference scheme. Regular grid was used for whole domain and the distance between nodes are shown by $\Delta x$ and $\Delta y$ in the $x$- and $y$-directions, respectively. The iteration process is terminated when the following condition is satisfied

$$\sum_{i,j}\left|\phi_{i,j}^{m} - \phi_{i,j}^{m-1}\right| \Big/ \sum_{i,j}\left|\phi_{i,j}^{m}\right| \leqslant 10^{-5} \tag{16}$$

where $m$ denotes the iteration step and $\phi$ stands for either $\theta_f$, $\theta_s$ or $\Psi$.

Table 2
Results for $Ra = 100$ to compare present results with literature

| Inclination angle of the side wall ($\gamma$) | 15° | 30° | 45° |
|---|---|---|---|
| $Nu_m$ (Baytas and Pop [33]) | 2.95 | 2.62 | 2.23 |
| $Nu_m$ (present) | 2.872 | 2.585 | 2.217 |

### 5.1. Validation

Due to lack of suitable experimental results in the literature pertaining to the present configuration, the obtained numerical results have been validated against the existing results for a square cavity filled with a porous medium. Thus, a first comparison for the mean Nusselt number $Nu$, as defined by Eq. (11b), with those from the open literature has been made for a value of $Ra = 1000$. These results can be found in our earlier two publications, Varol et al. [31,32]. We made also a second comparison using the entropy generation results reported by Baytas [24]. Comparison was performed with entropy generation due to heat transfer irreversibility and total entropy generation as shown in Fig. 2(a) ($Ra = 100$) and Fig. 2(b) ($Ra = 1000$). As can be seen from this comparison the obtained results show extremely good agreement with those from the literature. A third test was also performed to show validation of the numerical code with that from the literature. The comparison is given in Table 2. Results are compared with those of Baytas and Pop [33] which is obtained for a parallelogram geometry filled with a fluid saturated porous medium at different inclination angles of the side wall. As can be seen from Table 2 the difference between the present results and those from the literature is maximum 0.5%. Finally, we made another test for our code with the study by Saeid [34] which is performed for the problem of conjugate natural convection in a porous square enclosure. Results are shown by streamlines and isotherms contour plots in Fig. 3. All tests show that the results obtained using the present code give good agreement with those from the literature and it can be used with great confidence for further calculations.

## 6. Results and discussion

Entropy generation due to conjugate natural convection in a thick-walled right-angle trapezoidal enclosure filled with a porous medium has been numerically studied here. The govern-

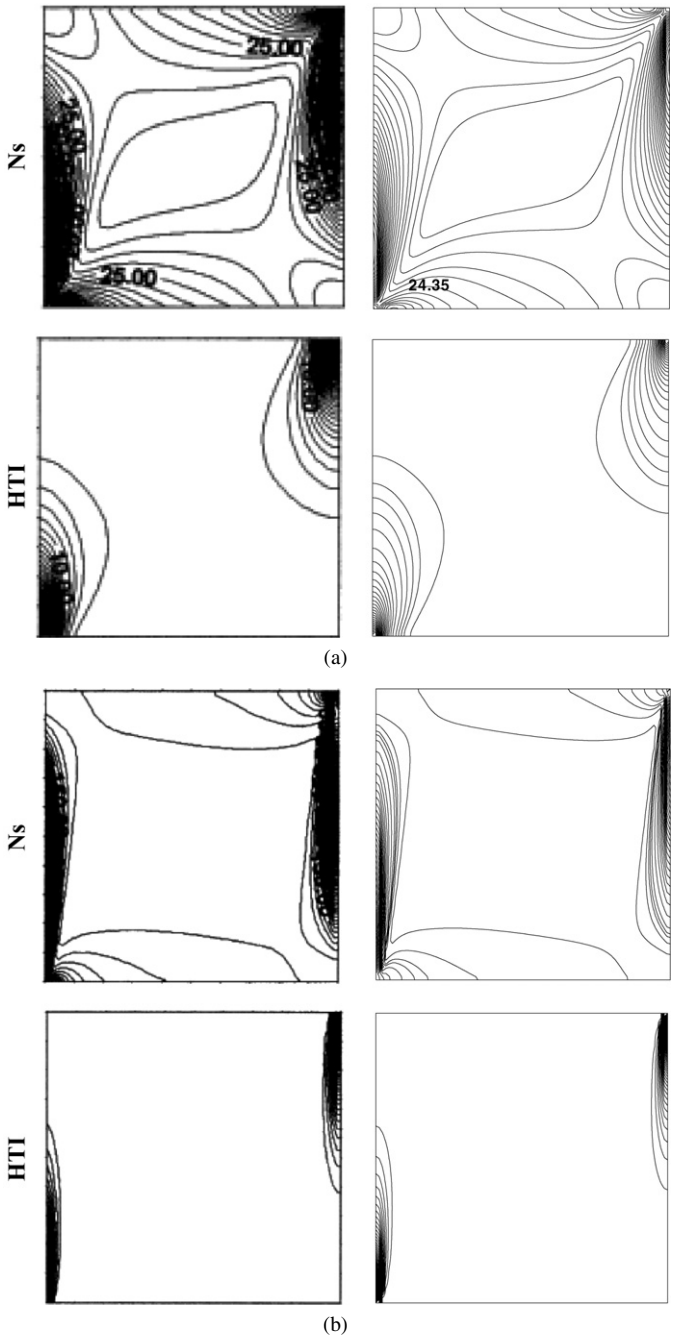


Fig. 2. Comparison of the total entropy generation number ($N_s$) and entropy generation due to HTI contours obtained with those of Baytas [24] (on the left) and present code (on the right), (a) $Ra = 100$, (b) $Ra = 1000$.

ing parameters are: Rayleigh number, $Ra = 50$, 500 and 1000, dimensionless thickness of the solid vertical wall, $S = 0.05$, 0.1 and 0.2, thermal conductivity ratio, $k = 0.1$, 1.0 and 10, inclination angle of the inclined wall, $\gamma = 35°$, 45° and 60°. We will first present results for the flow field with streamlines, temperature fields by isotherms and heat transfer by local and mean Nusselt numbers, then we will present results for the entropy generation due to HTI, the entropy generation due to FFI, iso-Bejan lines and Bejan number, respectively.

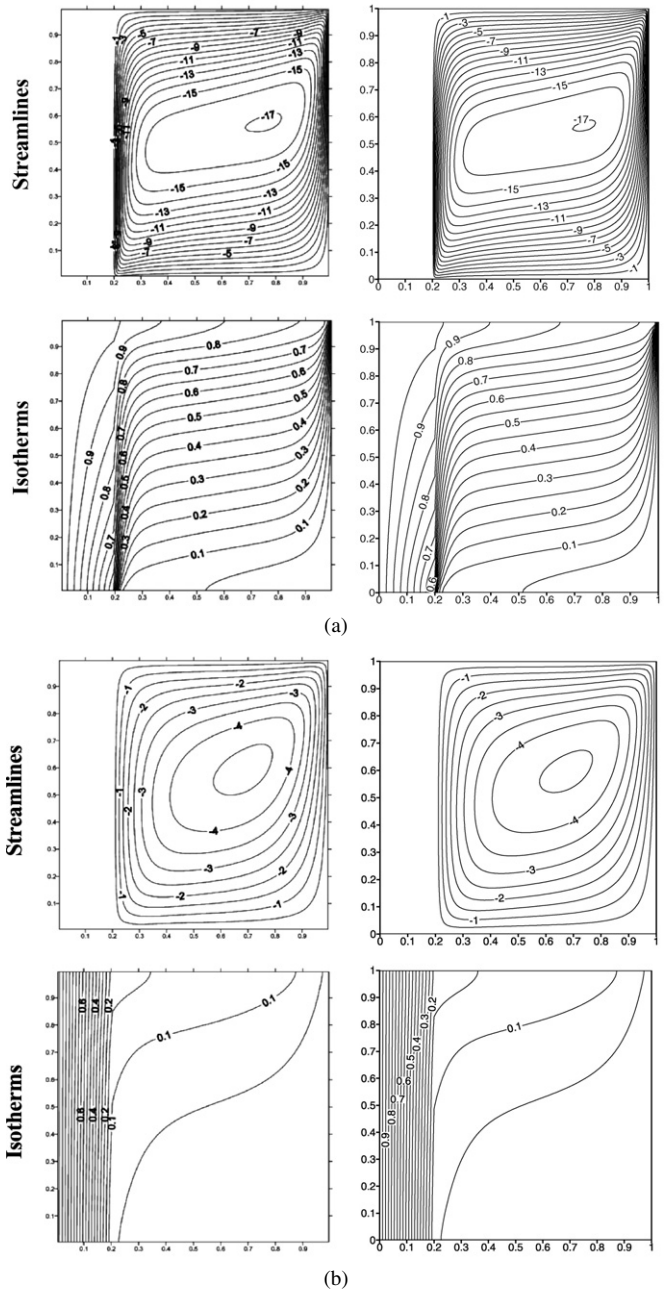


Fig. 3. Comparison of streamlines and isotherms contours obtained with those of Saeid [34] (on the left) and present study (on the right) for $Ra = 1000$, (a) $k = 10$, (b) $k = 0.1$.

### 6.1. Flow fields, temperature and entropy generation distributions

Fig. 4 shows streamlines (on the left) and isotherms (on the right) for different values of the Rayleigh number and $S = 0.1$, $k = 1.0$ and $\gamma = 45°$. It can be observed that the flow is unicellular for all values of Rayleigh numbers considered. For low Rayleigh numbers, isotherms are almost parallel to each other. This indicates that the conduction mode of heat transfer is dominant inside the porous region as shown from Fig. 4(a). Thus, circle shaped single cell was formed in clockwise cir-

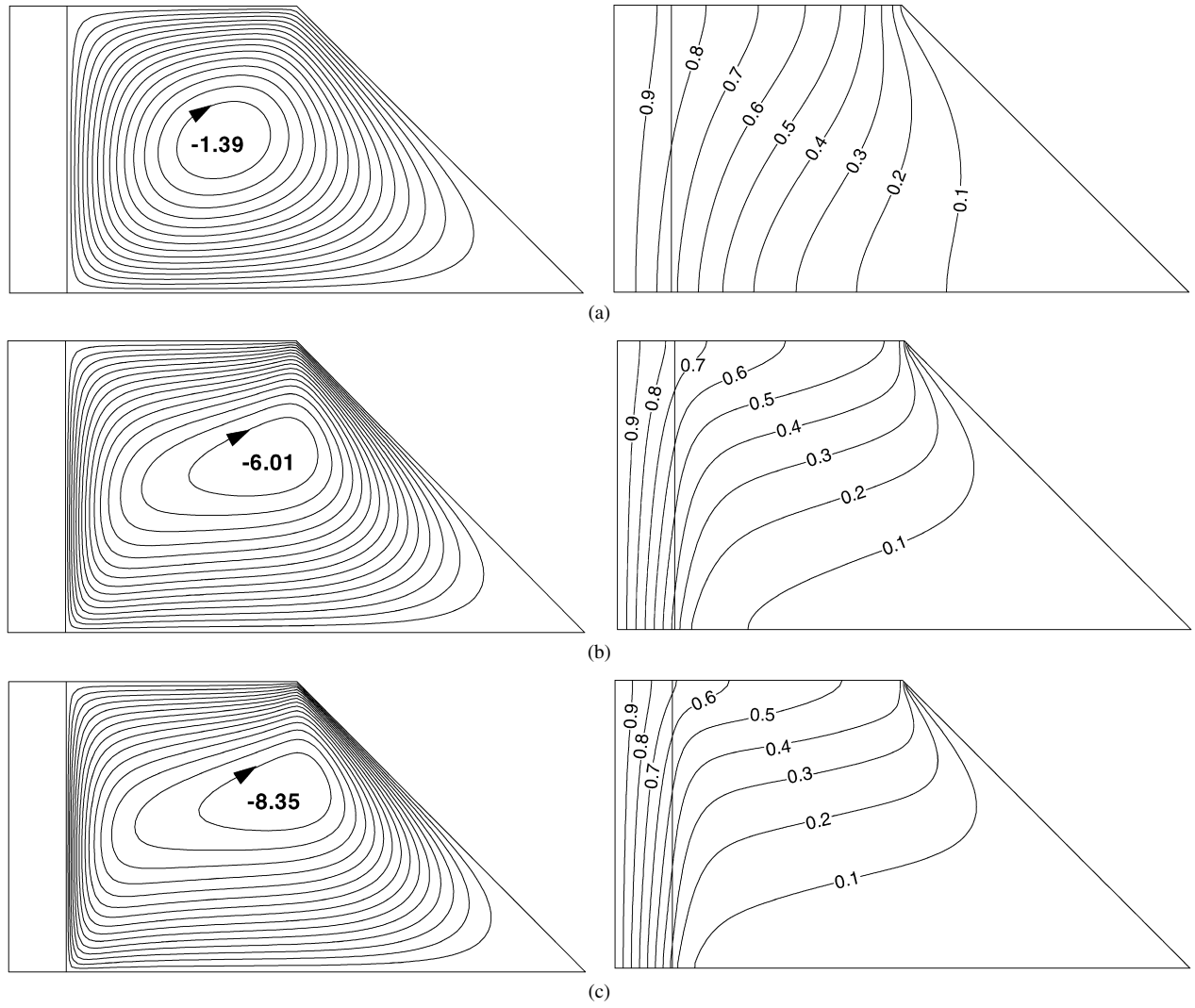


Fig. 4. Streamlines (on the left) and isotherms (on the right) for $S = 0.1$, $k = 1.0$ and $\gamma = 45°$ for different Rayleigh numbers, (a) $Ra = 50$, (b) $Ra = 500$, (c) $Ra = 1000$.

culation direction with $\Psi_{\min} = -1.39$. The Rayleigh number enhances the flow strength and oval shaped circulation cells were formed (Fig. 4(b)). In other words, convection becomes dominant for increasing Rayleigh number. The center of unicellular cell moves towards to the right top corner with increasing Rayleigh number. The right top corner plays effective role on both flow and temperature distribution especially at high Rayleigh numbers. Heated fluid circulates in clockwise rotation and it impinges to the top of the inclined wall and it stratifies into the porous area. In this way, the fluid accelerates with increasing Rayleigh number. Volume of the cold part of the fluid inside the right bottom corner increases with increasing Rayleigh number as seen from isotherms in Fig. 4 (b) and (c). The isotherm plots show that the temperature gradient within the solid wall increases with increasing Rayleigh number.

The entropy generation due to FFI and HTI are calculated with Eq. (13) using converged values of streamfunction and temperature. Results for entropy generation contours due to FFI (on the left) and HTI (on the right) are shown in Fig. 5 for the same governing parameters given in Fig. 4. Using of entropy generation distribution, we can obtain information about the active sides inside the enclosure and solid wall and main contributors for entropy generation. Entropy generation due to HTI also give information about the heat transport through the inner side of the solid wall to the inclined wall of the trapezoidal enclosure. As it is shown in Fig. 5(a) the top right corner and middle of the top and bottom walls are the active sites which generates the entropy due to FFI. Thus, entropy generation spreads all over the cavity. Entropy generation concentrates at the right top corner and it extends further along with increasing Rayleigh number as seen from Fig. 5 (a)–(c) (on the right). This is due to increasing of heat transfer. It means that more heat is transported from these locations. Contours are almost parallel to the bottom wall for low Rayleigh numbers in solid wall but they show inclined trend with increasing Rayleigh number (Fig. 5 (b) and (c)). Entropy generation domain becomes smaller with increasing Rayleigh number due to boundary layer regime. Maximum values are given at the top right corner with bold numbers that entropy generation due to HTI and FFI increases with increasing Rayleigh number.

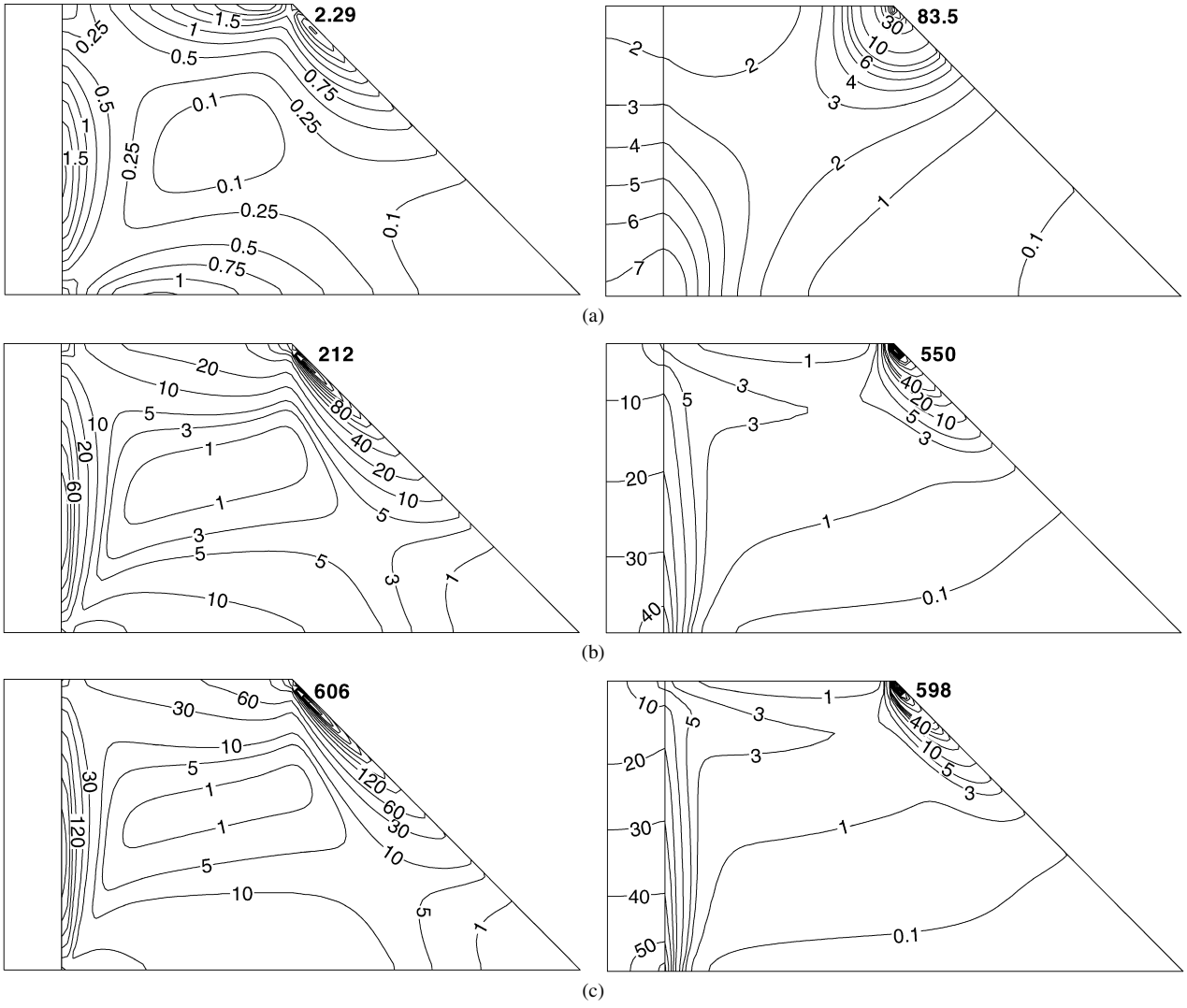


Fig. 5. Entropy generation due to fluid friction irreversibility (on the left) and heat transfer irreversibility (on the right) for $S = 0.1$, $\gamma = 45°$ and $k = 1.0$, (a) $Ra = 50$, (b) $Ra = 500$, (c) $Ra = 1000$.

Fig. 6 illustrates the effects of thermal conductivity ratio on streamlines and isotherms for $S = 0.1$, $\gamma = 45°$ and $Ra = 1000$. As it results from this figure, the thermal conductivity ratio of the solid wall to fluid inside the porous media is an effective parameter on both streamlines and isotherms. With the thermal conductivity ratio parameter is increased the flow strength also increases due to transport of more heat from the solid wall. For $k = 0.1$ (Fig. 6(a)), which corresponds to a low wall conductivity, the solid wall behaves as an insulation material and the results resemble those of the study by Saeid [34]. On the contrary, there is no obstacle for transfer of heat from outside to the porous media due to high conductivity ratio ($k = 10$). In this case, streamlines elongates diagonally inside the porous media. This result suggests that the thermal conductivity ratio can be a parameter to control heat and fluid flow.

Fig. 7 shows the streamlines (Fig. 7(a)) and isotherms (Fig. 7(b)), entropy generation due to FFI ((Fig. 7(c)) and entropy generation due to HTI (Fig. 7(d)) to examine the solid wall thickness on flow fields, temperature distribution and entropy generation for $k = 1.0$, $\gamma = 45°$ and $Ra = 1000$. Results are given for two values of the thickness of the solid wall as $S = 0.05$ (on the left) and $S = 0.2$ (on the right). As seen from these figures the wall thickness is an important parameter on streamlines since the flow strength decreases with increasing the thickness of the solid wall. The length of the main cell also decreases with increasing of wall thickness. The thickness of the wall directly affects the temperature distribution as given in Fig. 7(b). The thick wall behaves as a curtain for heat transport from outside of the thick wall to the fluid. The most flow region becomes cold due to the thick vertical wall. As presented in Fig. 7(c) the thickness of the wall mostly affects the entropy generation due to FFI. Concentration of entropy generation increases at the right top corner and its value decreases due to reduced heat transport with increasing of thickness of the solid wall. Because increasing of the thickness of solid wall, decreases the flow area and heat transfer is mostly occurred by conduction. Solid wall thickness mostly affects the inner flow domain due to decreasing of HTI with flow strength as illustrated in Fig. 7(d).

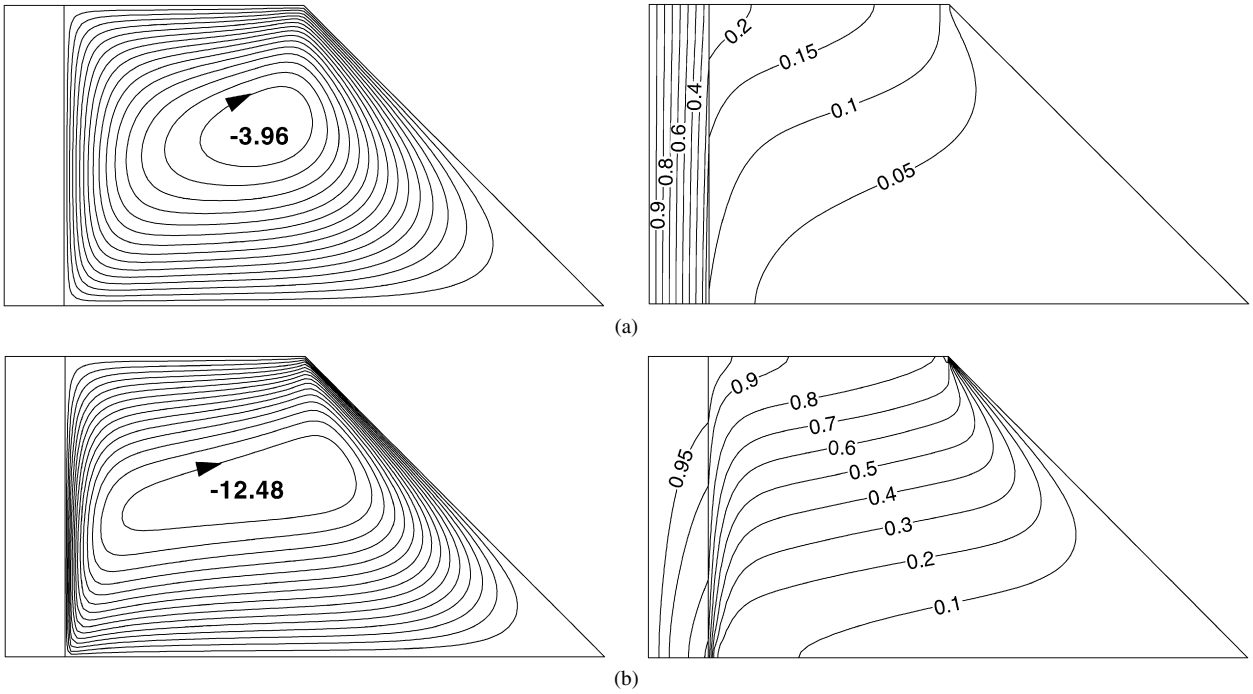


Fig. 6. Streamlines (on the left) and isotherms (on the right) for $S = 0.1$, $\gamma = 45^\circ$ and $Ra = 1000$, (a) $k = 0.1$, (b) $k = 10$.

Effects of inclination angle of the inclined wall on streamlines and isotherms and entropy generation are presented in Fig. 8 (a)–(d) for $\gamma = 35^\circ$ (on the left) and $\gamma = 60^\circ$ (on the right) at $S = 0.1$, $k = 1.0$ and $Ra = 1000$. For the smallest value of inclination angle, the cavity becomes shallower and diagonally elongated single cell was observed with $\Psi_{\min} = -8.42$ (Fig. 8(a)). However, absolute value of streamfunction is decreased with increasing of inclination angle. Isotherms become more parallel to the horizontal walls. However, temperature gradient inside the solid wall is also affected by the change of inclination angle as seen from Fig. 8(b). Entropy generation due to FFI and HTI inside the enclosure is also affected by the change of inclination angle of inclined wall as seen in Fig. 8 (c) and (d), respectively. Entropy generation due to FFI extends towards the middle of the porous region with increasing of volume of enclosure. Maximum entropy is decreased with increasing the inclination angle in both solid wall and the cavity. These figures clearly indicate that the geometry with sharp corner produces more entropy. It means that geometry is an important parameter on energy saving.

Iso-Bejan lines are plotted in Fig. 9 (a)–(c) for different inclination angles and two values of the Rayleigh numbers as $Ra = 50$ (on the left) and $Ra = 500$ (on the right). As we mentioned above the Bejan number is defined as ratio of entropy generation due to heat transfer irreversibility (HTI) to the total entropy generation ($N_s$). Thus, values of Bejan number changes between 0 and 1. As seen from Fig. 9 all corners of the cavity promote entropy generation. However, right bottom corner and intersection of inclined and top wall are stronger contributors for entropy generation. At the middle of the enclosure and at right corners, the entropy generation due to HTI becomes dominant at $Ra = 50$ (on the left of the Fig. 9). By increasing the Rayleigh number the fluid friction irreversibility becomes dominant at right corner at top region. It means that with the increasing of the Rayleigh number, entropy generation due to FFI becomes stronger. Fig. 9 also indicates that a diagonal pattern is observed and it becomes thinner with increasing of inclination of the enclosure (on the right of Fig. 9).

### 6.2. Heat transfer

Heat transfer is evaluated by local and mean Nusselt number as defined in Eqs. (11a) and (11b), respectively. Variation of the local Nusselt number along the interface of solid and fluid for different Rayleigh numbers and inclination angles is presented in Fig. 10 for $S = 0.1$ and $k = 1.0$. It is seen that values of local Nusselt number increases with increasing Rayleigh number due to increasing of incoming energy into the system. Their values decrease from bottom to top almost linearly. But slope of local Nusselt number is small at $Ra = 50$ due to conduction dominated heat transfer. They also decrease with increasing of inclination angle due to increasing of volume of the enclosure. Further, Fig. 11 shows the variation of the local Nusselt number along the interface for different thermal conductivity ratios. It is seen that local Nusselt number is almost constant for low thermal conductivity ratio. In this case, the partition behaves as insulation material. However, values of local Nusselt number increases with increasing of thermal conductivity ratio due to increasing of energy transport. For the case of $k = 10$, there is a low value of the local Nusselt number near the top of the vertical wall due to decreasing of distance between hot and cold walls. Fig. 11 also indicates that inclination angle is only an effective parameter for high conductivity ratio as $k = 10$. For lower values of conductivity ratio parameter it becomes insignificant.

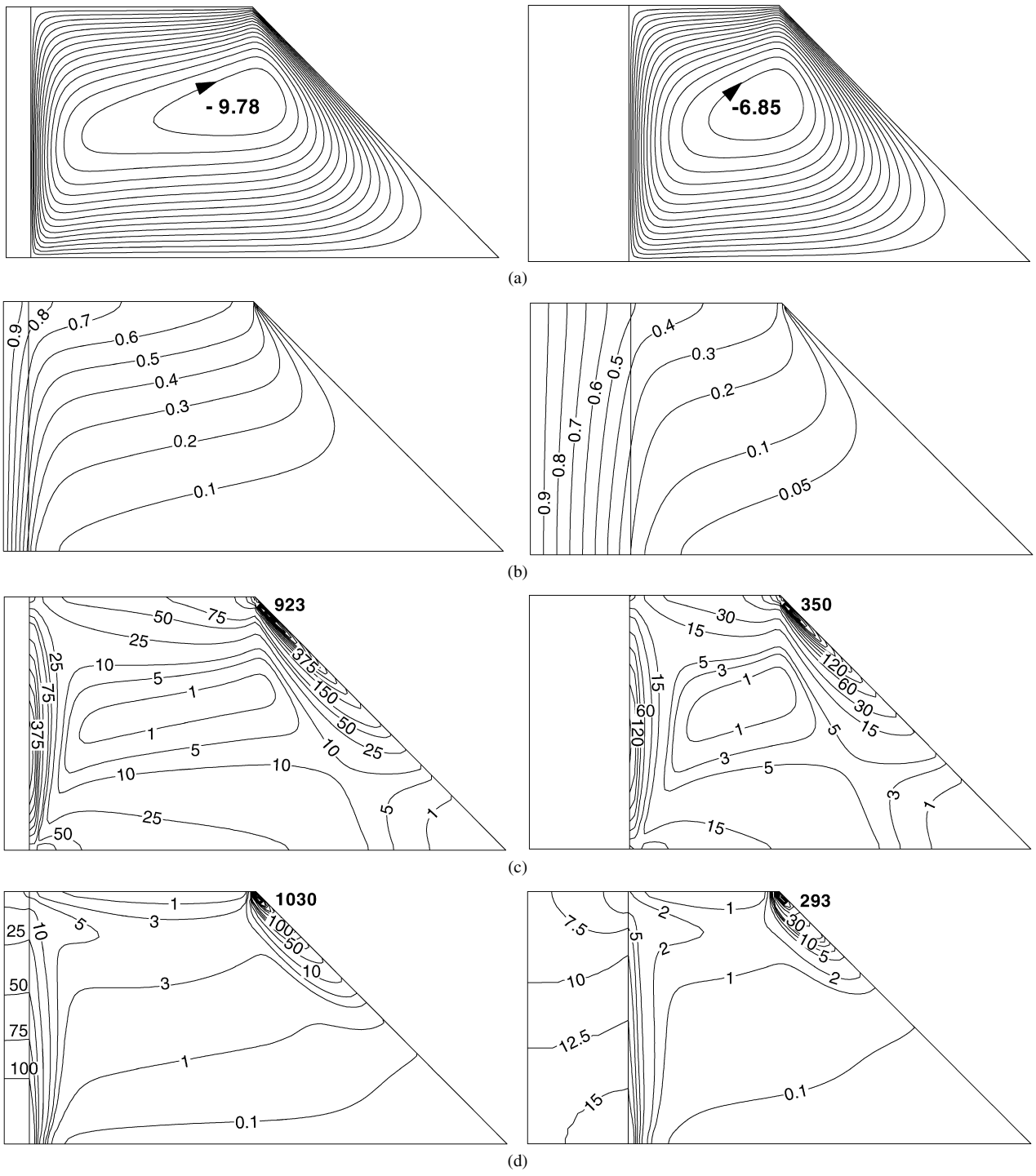


Fig. 7. (a) Streamlines, (b) Isotherms, (c) entropy generation due to FFI, (d) entropy generation due to HTI at $Ra = 1000$, $k = 1.0$, $\gamma = 45°$ for $S = 0.05$ (on the left) and $S = 0.2$ (on the right).

Effects of thickness of the solid wall on local Nusselt number are illustrated in Fig. 12 for different inclination angle at $Ra = 1000$ and $k = 1.0$. As seen from the figure the local Nusselt number increases with decreasing of the wall thickness due to increasing of heat transport. Values are decreased linearly depends on the temperature gradients. The figure also indicates that the value of local Nusselt number will become constant with further increasing of the wall thickness. Therefore, the inclination angle is an effective parameter for the lowest value of wall thickness. We present results for the mean Nusselt number at different thermal conductivity ratio and inclination angle in Fig. 13 for $S = 0.1$. It can be seen that heat transfer increases with increasing of thermal conductivity ratio and Rayleigh number. But it decreases with increasing of inclination angle. The values of mean Nusselt number all coincide for $k = 0.1$ due to insulating behavior of the solid wall. However, thermal conductivity values become effective on heat transfer only for $k > 1.0$ due to increasing of domination of convection

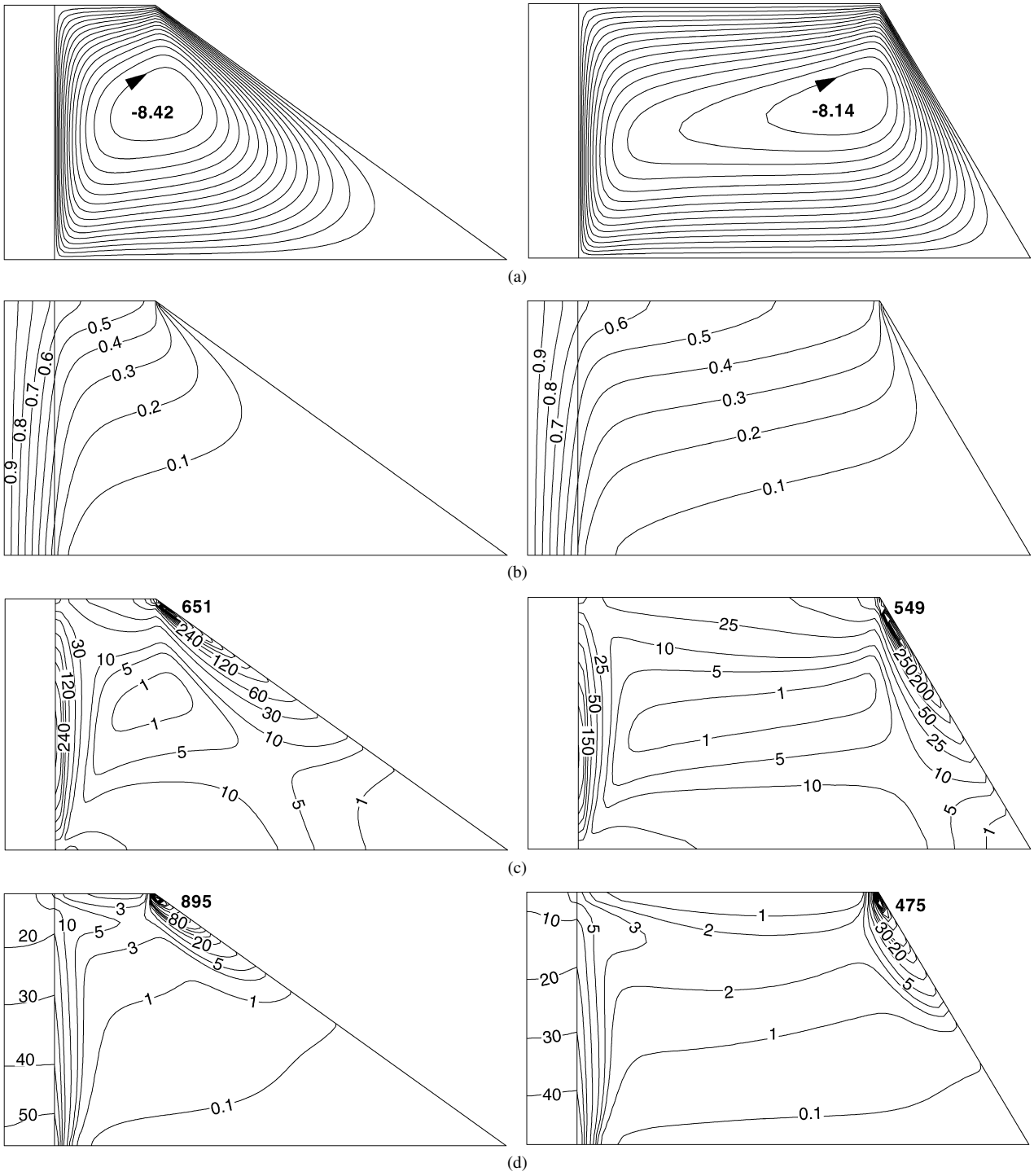


Fig. 8. (a) Streamlines, (b) isotherms, (c) entropy generation due to FFI, (d) entropy generation due to HTI at $Ra = 1000$, $k = 1.0$, $S = 0.1$ for $\gamma = 35°$ (on the left) and $\gamma = 60°$ (on the right).

mode of heat transfer. Conduction also becomes effective for whole domain at $Ra = 50$ as seen from Fig. 13. Heat transfer decreases with increasing the values of inclination angle due to long distance from hot and cold walls. Further, Fig. 14 presents the variation of mean Nusselt number with Rayleigh numbers at different wall thicknesses and inclination angles for $k = 1.0$. This figure indicates that there is little difference among mean Nusselt numbers for higher values of wall thickness and low Rayleigh numbers due to conduction dominated regime. On the contrary, the difference increases with increasing Rayleigh number and decreasing of wall thicknesses. The figure also shows that mean Nusselt number becomes constant for higher values of wall thickness. For higher values of wall thickness, variation of inclination angle on the mean Nusselt number becomes insignificant and heat transfer increases with decreasing of inclination angle.

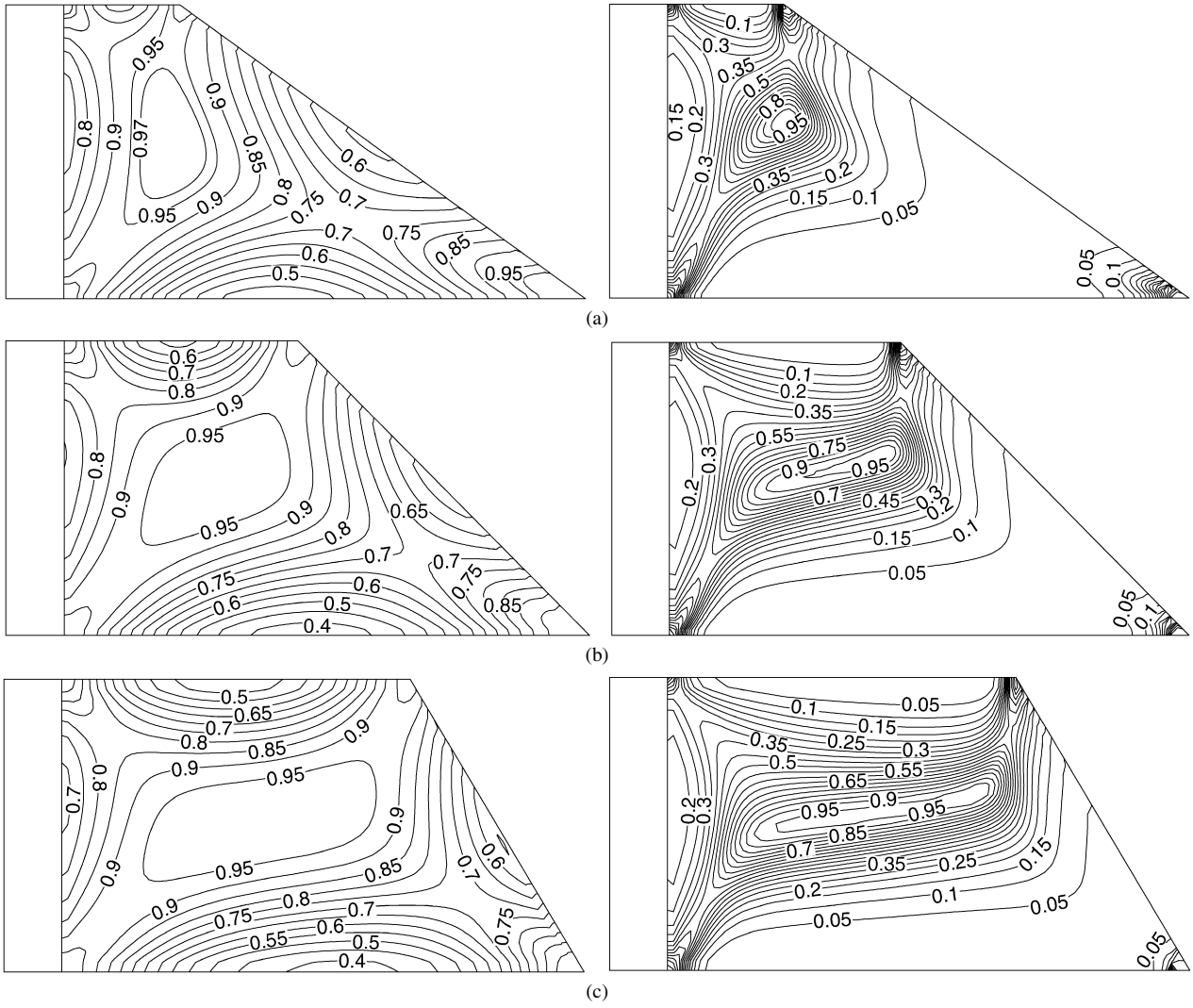


Fig. 9. Iso-Bejan lines at $Ra = 50$ (on the left) and $Ra = 500$ (on the right) for $S = 0.1$, $k = 1.0$, (a) $\gamma = 35°$, (b) $\gamma = 45°$, (c) $\gamma = 60°$.

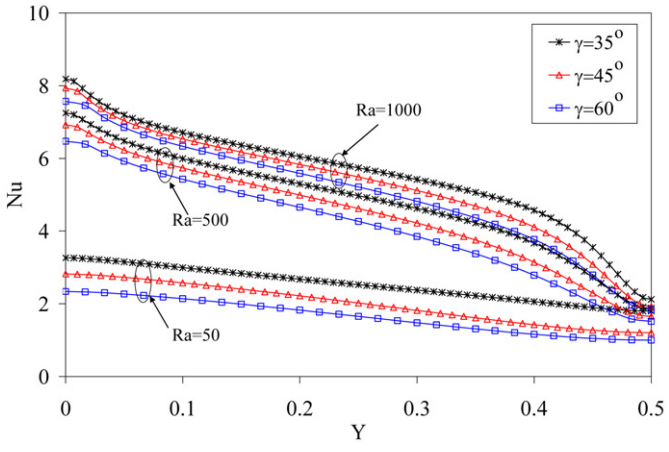


Fig. 10. Variation of local Nusselt number along the vertical interface for different Rayleigh numbers and inclination angles at $S = 0.1$ and $k = 1.0$.

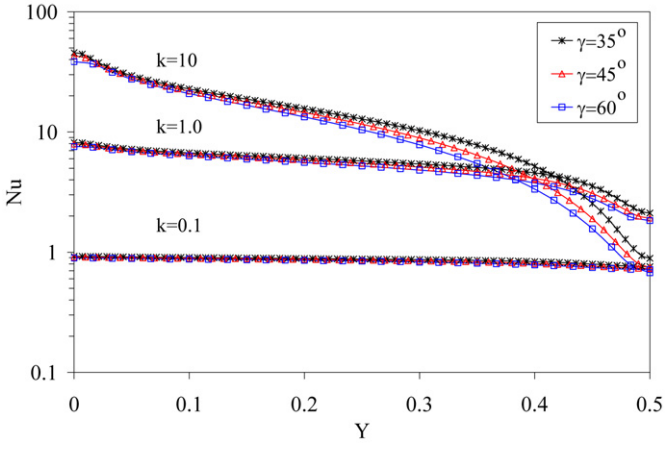


Fig. 11. Variation of local Nusselt number along the vertical interface for different thermal conductivity ratios and inclination angles at $Ra = 1000$ and $S = 0.1$.

### 6.3. Bejan number and total entropy generation

As it is well known the Bejan number ($Be$) is the ratio between the heat transfer irreversibility and the total irreversibility due to heat transfer and fluid friction. It is defined by Eq. (15). The value of $Be = 1$ is the limit at which the heat transfer irreversibility dominates, $Be = 0$ is the opposite limit at which the irreversibility is dominated by fluid friction effects and

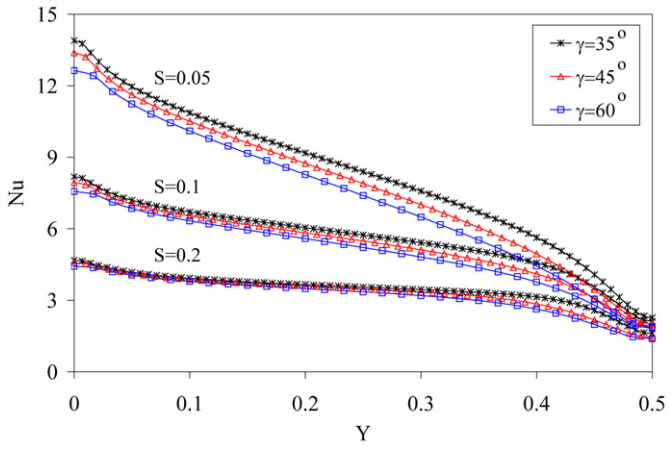


Fig. 12. Variation of local Nusselt number along the vertical interface for different thicknesses of the solid wall and inclination angles at $Ra = 1000$ and $k = 1.0$.

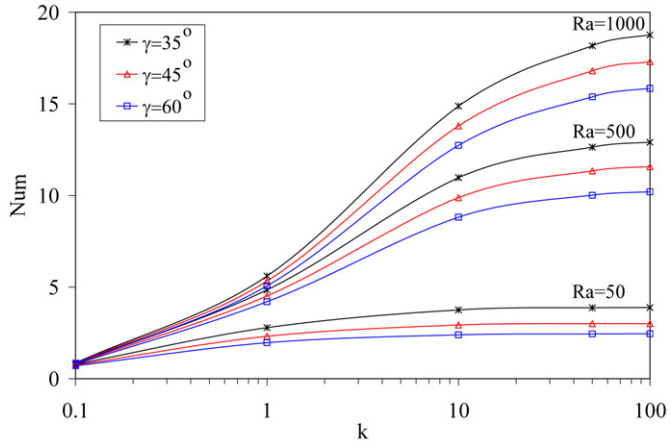


Fig. 13. Variation of mean Nusselt number with thermal conductivity ratio for different Rayleigh numbers and inclination angles at $S = 0.1$.

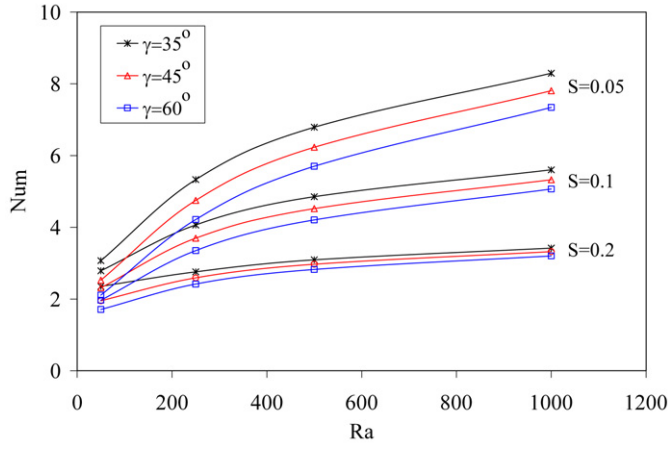


Fig. 14. Variation of mean Nusselt number with Rayleigh number for different thicknesses of the solid wall and inclination angles at $k = 1.0$.

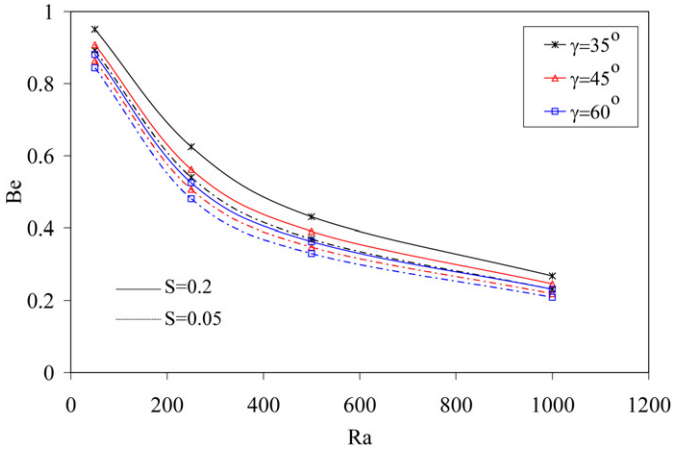


Fig. 15. Variation of Bejan number with Rayleigh number for different thicknesses of the solid wall and inclination angles at $k = 1.0$.

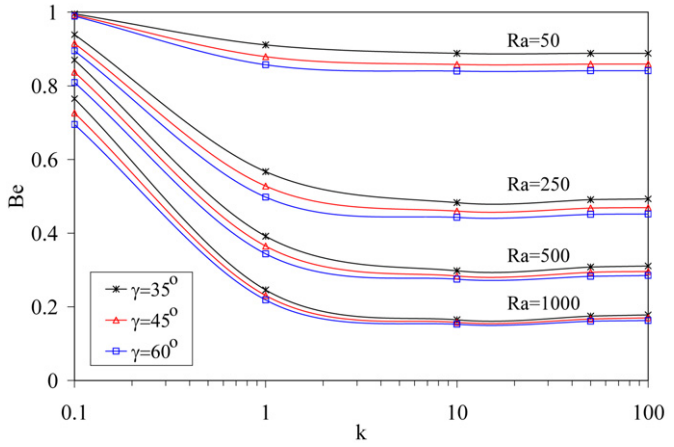


Fig. 16. Variation of Bejan number with thermal conductivity ratio for different Rayleigh numbers and inclination angles at $S = 0.1$.

$Be = 0.5$ is the case in which the heat transfer and fluid friction entropy production rates are equal (Varol et al. [28]). In this context, the variation of Bejan number with Rayleigh number for different thickness of the vertical wall and inclination angle at $k = 1.0$ is plotted in Fig. 15. This figure shows that the Bejan number decreases with decreasing of wall thickness due to increasing of domination of convection mode of heat transfer. Increasing of Rayleigh number again decreases the Bejan number. Higher values of $Be$ are obtained for lower values of inclination angle. It also decreases with increasing of inclination angle due to decreasing of entropy generation. However, Bejan number becomes constant for higher values of thermal conductivity ratio as shown in Fig. 16 for $S = 0.1$. In other words, higher value of thermal conductivity is not an effective parameter on Bejan number. It becomes constant at $Ra = 50$ due to domination of both thermal conductivity and entropy generation owing heat transfer irreversibility. As indicated in Fig. 16 the Bejan number decreases with increasing of inclination angle at the same Rayleigh number.

Finally, we presented the variation of the overall entropy generation with the Rayleigh number at different inclination angle of the inclined wall in Fig. 17 at $k = 1.0$ and $S = 0.1$.

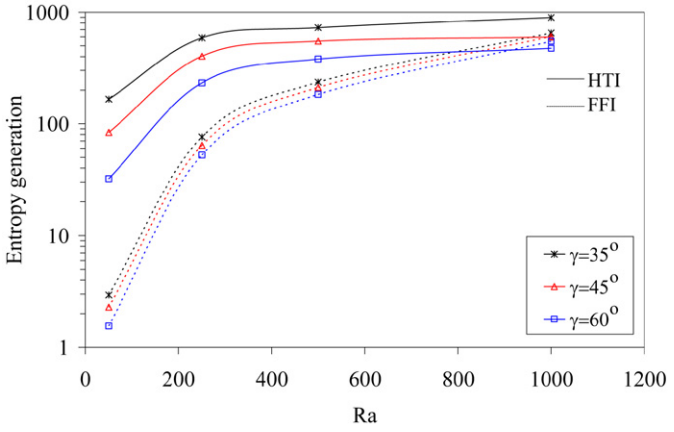


Fig. 17. Variation of entropy generation due to HTI and FFI with Rayleigh number for different inclination angles at $k = 1.0$ and $S = 0.1$.

The presentation was performed for both entropy generation due to HTI and FFI. The figure shows that variation of inclination angle has a more important role on HTI than that of FFI due to changing of distance between hot and cold walls. Their values are decreased with increasing of inclination angle. General observation shows that entropy generation increases with increasing Rayleigh number with the increasing of heat transfer and fluid friction irreversibility.

## 7. Conclusion

Entropy generation due to conjugate natural convection heat transfer in a thick walled right-angle trapezoidal enclosure filled with a fluid-saturated porous medium has been numerically performed using a finite difference method. Results are obtained for different Rayleigh numbers, thicknesses of the solid wall, inclination angles of inclined wall and thermal conductivity ratios. The main conclusions can be listed as follows:

(i) Both flow fields and temperature distributions are affected by the wall thickness, thermal conductivity ratio, inclination angle of the inclined wall and Rayleigh number.
(ii) Bejan number decreases with increasing Rayleigh number and thermal conductivity ratio. It becomes constant for higher values of thermal conductivities. Thermal conductivity ratio enhances the heat transfer. It becomes significant for $k > 1.0$ and high Rayleigh numbers.
(iii) Heat transfer increases with increasing Rayleigh number and decreases with increasing the solid wall thickness. On the contrary, lower Bejan number is obtained for lower values of wall thickness.
(iv) Main contributors for entropy generation are corners of the trapezoidal enclosures. Entropy generation due to HTI becomes stronger than that of entropy generation due to FFI at the center of the cavity. In other words, geometrical shape of the enclosure can be a control parameter from the point of view of energy saving.
(v) Inclination angle of the inclined wall becomes insignificant for lower value of thermal conductivity.

The study can be extended for higher Rayleigh numbers, unsteady and three-dimensional flows.

## Acknowledgements

The authors wish to express their very sincerely thanks to the reviewers for the valuable comments and suggestions.

## References

[1] D.A. Nield, A. Bejan, Convection in Porous Media, third ed., Springer, New York, 2006.
[2] D.B. Ingham, I. Pop (Eds.), Transport Phenomena in Porous Media, vol. III, Elsevier, Oxford, 2005.
[3] D.B. Ingham, A. Bejan, E. Mamut, I. Pop, Emerging Technologies and Techniques in Porous Media, Kluwer, Dordrecht, 2004.
[4] K. Vafai (Ed.), Handbook of Porous Media, second ed., Taylor & Francis, New York, 2005.
[5] T.S. Lee, Numerical experiments with fluid convection in tilted nonrectangular enclosures, Numer. Heat Transfer Part A 19 (1991) 487–499.
[6] B.V.R. Kumar, B. Kumar, Parallel computation of natural convection in trapezoidal porous enclosures, Math. Comput. Simulation 65 (2004) 221–229.
[7] A.C. Baytas, I. Pop, Natural convection in a trapezoidal enclosure filled with a porous medium, Int. J. Eng. Sci. 39 (2001) 125–134.
[8] F. Moukalled, S. Acharya, Natural convection in trapezoidal cavities with baffles mounted on the upper inclined surfaces, Numer. Heat Transfer Part A 37 (2000) 545–565.
[9] F. Moukalled, M. Darwish, Natural convection in a partitioned trapezoidal cavity heated from the side, Numer. Heat Transfer Part A 43 (2003) 543–563.
[10] M. Boussaid, A. Djerrada, M. Bouhadef, Thermosolutal transfer within trapezoidal cavity, Numer. Heat Transfer Part A 43 (2003) 431–448.
[11] J.T. Van Der Eyden, T.H. Van Der Meer, K. Hanjalic, E. Biezen, J. Bruining, Double-diffusive natural convection in trapezoidal enclosures, Int. J. Heat Mass Transfer 41 (1998) 1885–1898.
[12] S. Kumar, Natural convective heat transfer in trapezoidal enclosure of box-type solar cooker, Renewable Energy 29 (2004) 211–222.
[13] E. Papanicolaou, V. Belessiotis, Double-diffusive natural convection in an asymmetric trapezoidal enclosure: unsteady behavior in the laminar and the turbulent-flow regime, Int. J. Heat Mass Transfer 48 (2005) 191–209.
[14] Y. Varol, H.F. Oztop, I. Pop, Numerical analysis of natural convection in an inclined trapezoidal enclosure filled with a porous medium, Int. J. Thermal Sciences 47 (2008) 1316–1331.
[15] M. Peric, Natural Convection in trapezoidal cavities, Numer. Heat Transfer Part A 24 (1993) 213–219.
[16] M. Hammami, M. Mseddi, M. Baccar, Numerical study of coupled heat and mass transfer in a trapezoidal cavity, Eng. Appl. Comp. Fluid Dynamics 1 (2007) 216–226.
[17] A. Bejan, Entropy Generation through Heat and Fluid Flow, John Wiley & Sons, 1994.
[18] J.Y. San, W.M. Worek, Z. Lavan, Entropy generation in convective heat transfer and isothermal convective mass transfer, J. Heat Transfer 109 (1987) 647–652.
[19] M.A. Rosen, Second-law analysis: Approaches and implications, Int. J. Energy Res. 23 (1999) 415–429.
[20] U. Narusawa, The second-law analysis of mixed convection in rectangular ducts, Heat and Mass Transfer 37 (2001) 197–203.
[21] M. Mourad, A. Hassen, H. Nejib, B.B. Ammar, Second law analysis in convective heat and mass transfer, Entropy 8 (2006) 1–17.
[22] L.B. Erbay, Z. Altac, B. Sulus, An analysis of the entropy generation in a square enclosure, Entropy 5 (2003) 496–505.
[23] B.S. Yilbas, S.Z. Shuja, S.A. Gbadebo, H.I. Abu Al-Hamayel, K. Boran, Natural convection and entropy generation in a square cavity, Int. J. En. Res. 22 (1998) 1275–1290.
[24] A.C. Baytas, Entropy generation for natural convection in an inclined porous cavity, Int. J. Heat Mass Transfer 43 (2000) 2089–2099.

[25] M. Magherbi, H. Abbasi, A. Ben Brahim, Entropy generation at the onset of natural convection, Int. J. Heat Mass Transfer 46 (2003) 3441–3450.

[26] S. Mahmud, R.A. Fraser, Magnetohydrodynamic convection and entropy generation in a square porous cavity, Int. J. Heat Mass Transfer 47 (2004) 3245–3256.

[27] G. Ruocco, Entropy generation in conjugate heat transfer from a discretely heated plate to an impinging confined jet, Int. Comm. Heat Mass Transfer 24 (1997) 201–210.

[28] Y. Varol, H.F. Oztop, A. Koca, Entropy generation due to conjugate natural convection in enclosures bounded by vertical solid walls with different thicknesses, Int. Comm. Heat Mass Transfer 35 (2008) 648–656.

[29] P.M. Haese, M.D. Teubner, Heat exchange in an attic space, Int. J. Heat Mass Transfer 45 (2002) 4925–4936.

[30] H. Asan, L. Namli, Numerical simulation of buoyant flow in a roof of triangular cross-section under winter day boundary conditions, Energy & Buildings 33 (2001) 753–757.

[31] Y. Varol, H.F. Oztop, A. Koca, Entropy production due to free convection in partially heated isosceles triangular enclosures, Applied Thermal Engineering 28 (2008) 1502–1513.

[32] Y. Varol, H.F. Oztop, I. Pop, Numerical analysis of natural convection for a porous rectangular enclosure with sinusoidally varying temperature profile on the bottom wall, Int. Comm. Heat Mass Transfer 35 (2008) 56–64.

[33] A.C. Baytas, I. Pop, Free convection in oblique enclosures filled with a porous medium, Int. J. Heat Mass Transfer 42 (1999) 1047–1057.

[34] N.H. Saeid, Conjugate natural convection in a porous enclosure: effect of conduction in one of the vertical walls, Int. J. Thermal Sci. 46 (2007) 531–539.